ELSEVIER

Journal of Marine Systems 35 (2002) 249–268

JOURNAL OF MARINE SYSTEMS

www.elsevier.com/locate/jmarsys

Seasonal variation of the circulation in the Taiwan Strait

Sen Jan [a,*], Joe Wang [b,1], Ching-Sheng Chern [b,1], Shenn-Yu Chao [c,2]

[a] *Institute of Physical Oceanography, National Sun Yat-Sen University, 70 Lien-Hai Road, Kaohsiung 80424, Taiwan*
[b] *Institute of Oceanography, National Taiwan University, P.O. Box 23-13, Taipei 10617, Taiwan*
[c] *Horn Point Laboratory, University of Maryland Center for Environmental Science, P.O. Box 0775, Cambridge, MD 21613-0775, USA*

Received 4 February 2000; accepted 20 February 2002

Abstract

The Taiwan Strait is an essentially meridional channel connecting the East and South China Seas. There is often a northward current on the east side and a southward current on the west side. The source water feeding the eastern boundary current is South China Sea Water in summer and Kuroshio Branch Water in other seasons. The current on the west side carries colder and fresher China Coastal Water southward. Both currents are modulated by the annual cycle of monsoon wind forcing, which reinforcesthe northward current in summer but southward current in other seasons. Further, both currents are partially impeded by a bottom ridge (Changyun Rise) in the middle reaches of the strait. The combination of monsoon and topography forcing leads to the winter blocking of northward current, spring renewal of northward intrusion, minimal blocking of northward intrusion in summer, and fall emergence of China Coastal Current. A recent hydrographic data set, satellite images and a numerical model lend support to these findings.

Keywords: Taiwan Strait; Circulation; Seasonal variation; Numerical model

1. Introduction

The Taiwan Strait (hereafter TS), bounded by the China continent to the west and the island of Taiwan to the east, is a shallow strait about 180 km wide, 350 km long and 60 m in average depth (Fig. 1). Waters in the South and East China Seas are exchanged through the strait. Further, the northward flowing Kuroshio Current hugging the east coast of Taiwan often branches into the TS and intrudes northward (Chuang, 1985, 1986; Wang and Chern, 1988). Much farther to the north, it is often speculated that the origin of the Tsushima Current entering the Sea of Japan may be linked to the current coming out of the TS (Fang et al., 1991; Isobe, 1999). Thus, circulation in the TS transcends regional importance.

Winds over the TS are dominated by the East Asia monsoon, from northeast in winter and from southwest in summer. Fig. 2 shows monthly mean wind stress vectors averaged from 1986 to 1995 derived from a weather station south of Penghu Island (DG in Fig. 1). The northeast monsoon begins in mid-September, peaks from October to January, and weakens continuously thereafter. By comparison, the southwest monsoon in June and July is much weaker.

* Corresponding author. Tel.: +886-7-5252000x5353; fax: +886-7-5255359.
E-mail addresses: senjan@mail.nsysu.edu.tw (S. Jan), wang@oc.ntu.edu.tw (J. Wang), chern@ipx.oc.ntu.edu.tw (C.-S. Chern), chao@hpl.umces.edu (S.-Y. Chao).
[1] Tel.: +886-2-23623751; fax: +886-2-23626092.
[2] Tel.: +1-410-221-8200; fax: +1-410-221-8490.

0924-7963/02/$ - see front matter
PII: S0924-7963(02)00130-6

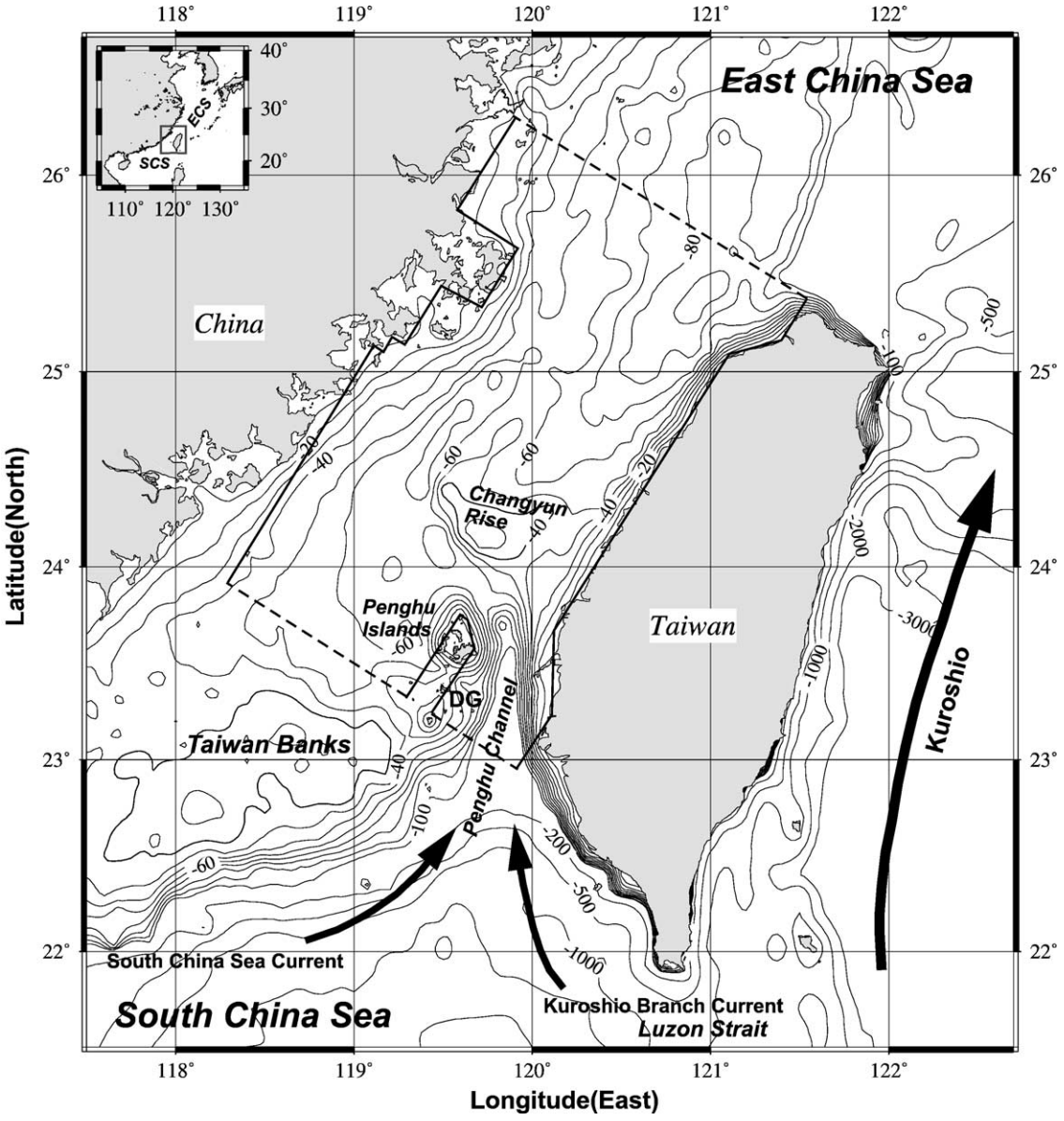

Fig. 1. Isobaths (in meters) in and around the Taiwan Strait. The small insert at the upper-left corner shows the location of Taiwan Strait relative to the East China Sea (ECS) and the South China Sea (SCS). The dashed and solid lines indicate open-ocean and land boundaries of the model domain, respectively.

The cold war era has resulted in the lack of flow transport estimates through the TS. Using limited hydrographic and sea level data, Wyrtki (1961) suggested that the transport is 0.5–1 Sv northward in summer and 0.5 Sv southward in winter. Leaving mesoscale variability aside, the overall circulation patterns inside the strait have been suggested for some time. Fig. 3 is Ninno and Emery's (1961) view of summer and winter circulation patterns. The surface flow charts compiled by Nitani (1972) are similar. In summer, the pattern suggested that both Kuroshio Branch Water and South China Sea Water intrude

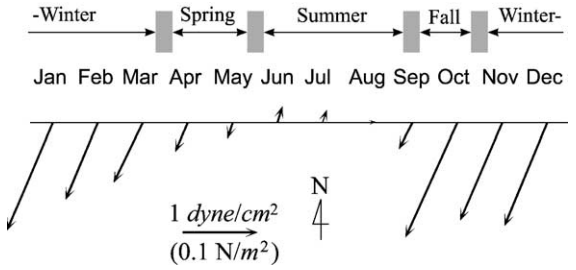

Fig. 2. Stick diagram of monthly mean wind stresses averaged over ten years (1986–1995) at a location south of the Penghu Islands (DG in Fig. 1).

northward. On eastern side, the northeastward mean current in summer can be as strong as 90 cm/s according to Nitani (1972). The southwest monsoon is quite weak in summer, typically weaker than 0.025 N/m^2. Such weak wind forcing cannot drive a current as strong as 90 cm/s. Thus, a good portion of the circulation must be forced by remote forcing of large-scale origin rather than by local winds. The large-scale forcing is set up in such a way that it forces waters in the northern South China Sea to flow northward and enter the East China Sea through the TS. In winter, the China Coastal Current on the western side is driven by the northeast monsoon, while the windward Kuroshio Branch Current on eastern side is remotely driven, having a reduced northward speed of about 20 cm/s. Guan (1994) and Huang et al. (1994) also emphasized that a northward current is a year-round feature, connecting the South China Sea Warm Current to the south and the Taiwan Warm Current to the north of the strait. The circulation patterns as depicted in Fig. 3 are oversimplified. In reality, topographic features in the strait are expected to produce considerable distortion to the circulation. In fact, the main objective of this paper is focused on the topography-induced circulation in the strait.

The bathymetry in Fig. 1 suggests sizable topographic blocking of throughflows in the strait. Southwest of the TS, the Taiwan Banks (or Formosa Banks) with depths ranging from 20 to 40 m partially blocks the passage to the South China Sea. In the southeast corner of the TS, the deep Penghu Channel guides the intruding Kuroshio Branch Water or South China Sea Water northward. North of Penghu Channel is the Changyun Rise (CYR), partially blocking along-strait transport on eastern side of the strait. North of CYR, the water deepens again on eastern side of the strait.

Early hydrographic measurements by Chu (1971), although sparse, identified three water masses in the strait: the Kuroshio Branch Water (KBW) with high temperature and high salinity, the China Coastal Water (CCW) with low temperature and low salinity, and the South China Sea Water (SCSW) with intermediate temperature and salinity. In terms of air–sea heat exchange, the maximum monthly heat loss occurs in

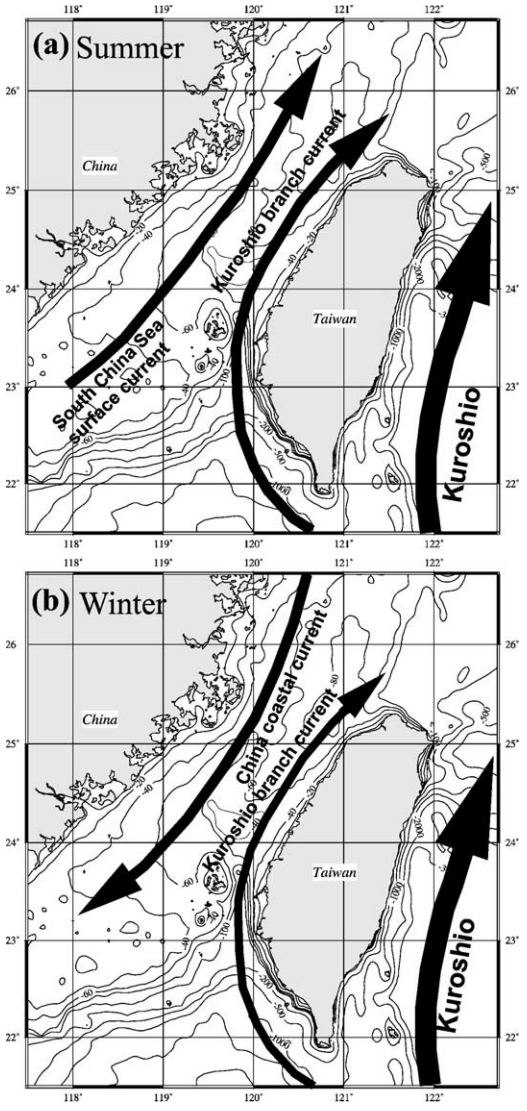

Fig. 3. Early views of the Taiwan Strait circulation in (a) summer and (b) winter, after Ninno and Emery (1961) and Nitani (1972).

December or January, while the sea gains heat almost uniformly everywhere in summer (Ishii and Kondo, 1987; Hirose et al., 1999; Na et al., 1999). According to Hirose et al. (1999), the strait water loses heat to the atmosphere at the rates of 220, 30 and 170 W/m^2 in winter, spring and fall, respectively, and gains heat at a rate of 130 W/m^2 in summer. The seasonal variation is largely dictated by the strength of cold northeast monsoon in winter. When averaged over a year, the strait water as a whole loses heat to the atmosphere. Since the water temperature is higher to the south, the heat loss to the atmosphere must be replenished by northward intrusion of warm waters from the south. Thus, Wyrtki's (1961) estimates of volume transports are plausible to lowest order, in the sense that his estimated transport is northward when averaged over a year.

Historical hydrographic data before 1980 are too scanty in space and time to reveal mesoscale features and seasonality of the strait circulation. Fortunately, available data have increased exponentially since 1980. Further, previously unavailable sea surface temperature (SST) images from satellites also emerge as an important diagnostic tool. The new data, to be discussed below, help identify topography-induced mesoscale features in the strait. A numerical model is then presented to reproduce salient features revealed from observations. The hydrographic data set is sufficiently higher in spatial and temporal resolution than the global climatology data compiled in Levitus (1982). The data set is analyzed and presented below.

2. Hydrography and SST

Thirty CTD surveys were conducted between 1985 and 1992. Fig. 4 shows the distribution of the monthly cruise in this period. Each cruise covered about two thirds of the strait on the eastern side. In consequence, CTD data are somewhat scarce near the China coast. The satellite coverage of SST more or less compensated for the lack of hydrographic data on the western side. Data were sorted out by the season. For convenience, seasons are defined below according to changes in the monsoon. Winter, spring, summer and fall are defined as periods from November to March, April to May, June to August and September to October, respectively. The temporal resolution of this data set is inadequate to quantify interannual variations at the present time. However, global climatological data sets such as those of Kalnay et al. (1996) indicated that the interannual changes are small in the strait. For this reason, fields are displayed below on a one-per-season basis regardless of the year. Note that the spatial coverage of hydrographic surveys varies from cruise to cruise. The choice of particular surveys for illustrations is not only to highlight seasonal variations, but also to maximize spatial coverage in the strait proper.

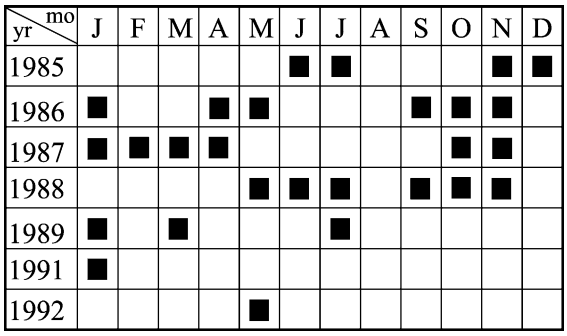

Fig. 4. Distribution of monthly CTD survey cruises from 1985 to 1992.

Fig. 5 illustrates typical near-surface and near-bottom features of temperature and salinity fields in winter (upper-left panels), spring (upper-right panels), summer (lower-left panels) and fall (lower-right panels). Observations were made in November 12–16 of 1988, April 22–24 of 1986, June 7–10 of 1988, and September 1–6 of 1988. Near-surface features are displayed at 10 m depth. Deep features are illustrated at 50 m depth or bottom if the water depth is less than 50 m. Contour intervals are 0.5 °C for temperature and 0.1 psu for salinity. Further, the contours are derived from an observation network with a longitudinal resolution of 1/6 and a latitudinal resolution around 1/3 degree. Fig. 6 shows four SST images received on January 19 of 1999, April 13 of 1999, June 24 of 1999, and October 1 of 1998, illustrating typical patterns in four seasons.

2.1. Winter blocking

Under the peak northeast monsoon, winter temperature and salinity fields (Fig. 5a) suggest a blocked circulation pattern. At 10 m depth, colder (<22 °C)

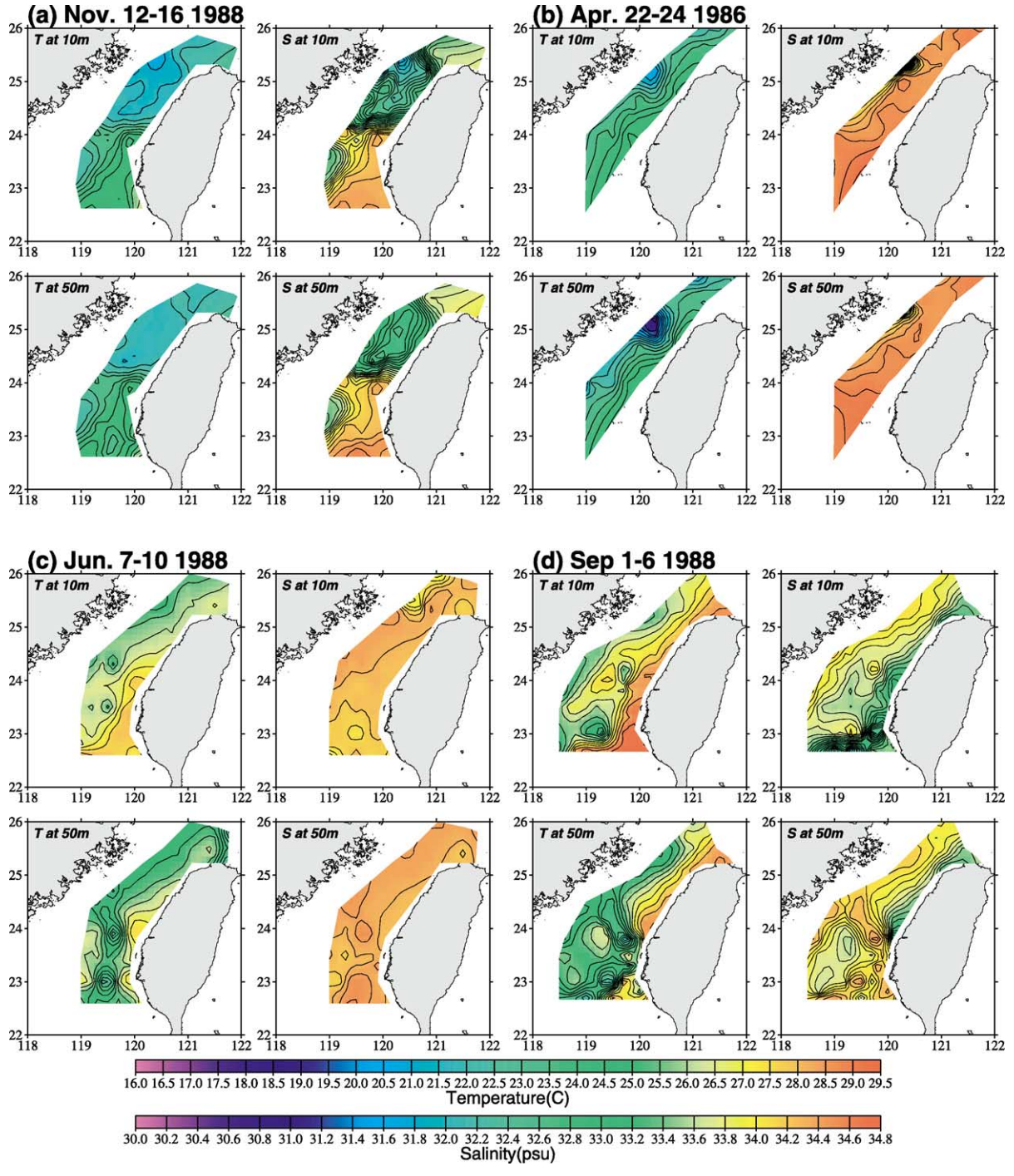

Fig. 5. Temperature and salinity distributions at 10 and 50 m depths for (a) winter, (b) spring, (c) summer and (d) fall. The CTD data were acquired in November 12–16 1988, April 22–24 1986, June 7–10 1988 and September 1–6 1988, respectively.

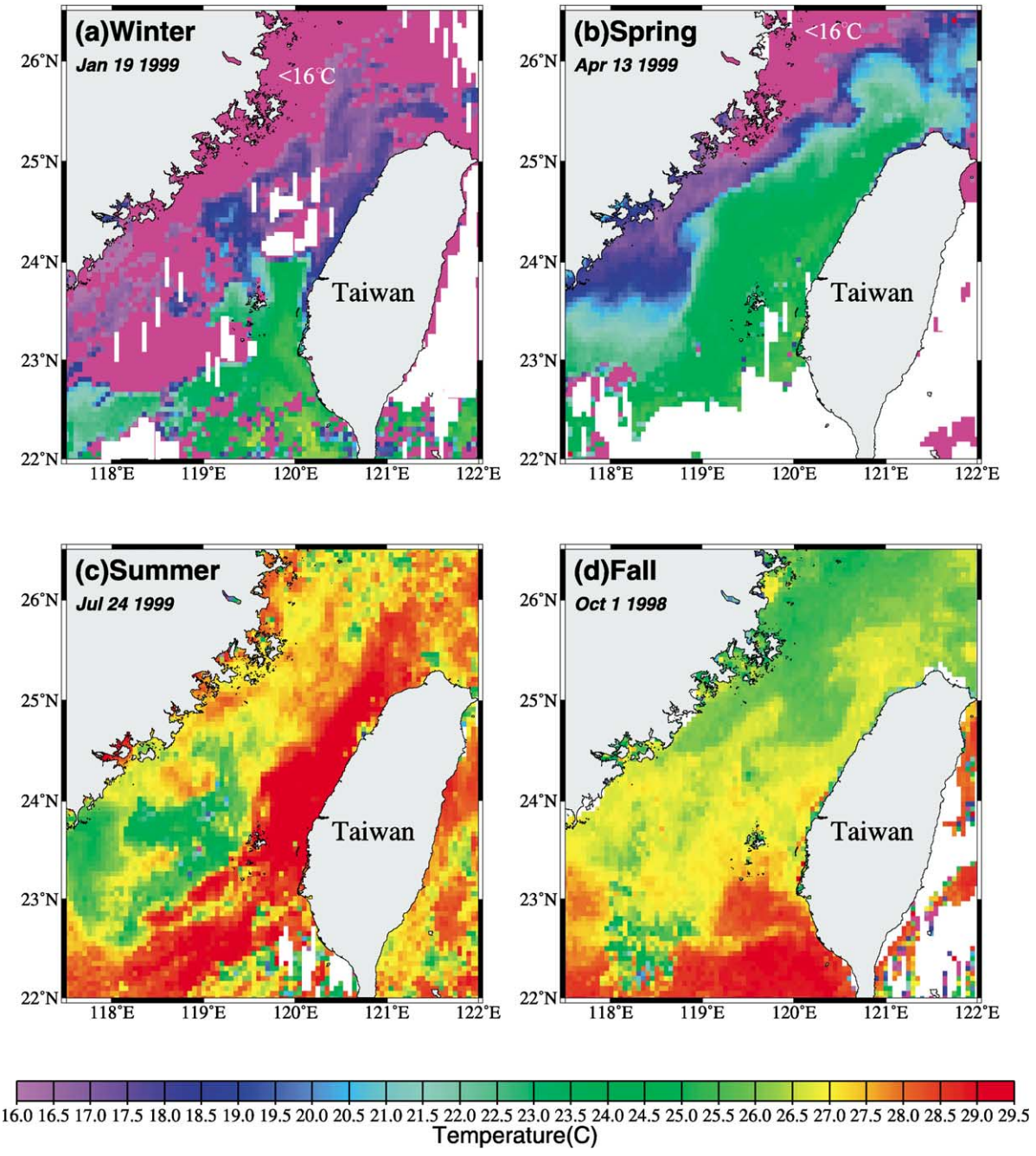

Fig. 6. Sea surface temperature images in (a) winter, (b) spring, (c) summer and (d) fall. The SST images were taken on January 19 1999, April 13 1999, July 24 1999 and October 1 1998, respectively.

and fresher (<33 psu) waters extend from China coast eastward and occupy the northern TS (Wang and Chern, 1989; China Ocean Press, 1992; Jan et al., 1998). In a larger scale setting, the SST image (Fig. 6a) suggests the northern cold anomaly is a southwestward extension of the China Coastal Water. Investigators on the western side of the TS often indicated that the southward-moving China Coastal Water can reach as far south as the north edge of the Taiwan Banks (Xiao and Cai, 1988). In the southeastern TS, warmer (>24 °C) and saline (>34 psu) waters are bounded in the Penghu Channel (Fig. 5a). The blocked water mass is distinctively Kuroshio Branch Water (Wang and Chern, 1988). Occasionally, a warm tongue may protrude northward from the northern end of the Penghu Channel (see Fig. 6a) when the northeast monsoon temporally weakened or diminished. Between northern and southern water masses, a zonal oceanic front over the CYR is usually observed in winter. The front is about 30 km wide; temperature and salinity differences across the front are about 2 °C and 1 psu, respectively. Temperature and salinity fields near the bottom layer showed similar patterns. Note also that the cold water overlies warm water in the northern TS. In consequence, vertical stratification is rendered stable by salinity rather than temperature.

2.2. Spring relaxation

The weakened northeast monsoon in spring leads to northward intrusion of once blocked Kuroshio Branch Water in Penghu Channel. Temperature and salinity vary little with depths. In other words, the stratification is mostly horizontal. Warm (>23 °C) and saline (>34.2 psu) waters originally trapped in Penghu Channel in winter expand northward over and beyond CYR (Figs. 5b and 6b). Consequently, the Kuroshio Branch Water covers the entire eastern half of the strait while the China Coastal Water is confined to the western side. Fig. 6b also indicates that the Kuroshio Branch Water broadens over Changyun Rise, narrowing once again north of CYR. Conceivably, the northward Kuroshio Branch Current may become diffuse or bifurcate over the ridge; this will be verified later using a numerical model. It is also worth noting that the salinity anomaly becomes much weaker in spring.

2.3. Minimum blocking in summer

Wind direction in this period changes from northeast to southwest (Fig. 2). The southwest monsoon wind prevails for only 2 months (June and July) and is much weaker than the winter northeast monsoon. Isotherms and isohalines in the upper layer (depth <20 m) follow the orientation of the TS, with warm and fresher waters to the east and cold and saline waters to the west (Wang and Chern, 1992; China Ocean Press, 1992). Near-bottom temperature and salinity fields in Fig. 5c show sizable deviation. Along the coast of Taiwan, the generally southwest–northeast-oriented isotherms are displaced seaward (westward) over and around CYR. Near-bottom isohalines also show similar tendency to a certain extent. In other words, cold (<24 °C) and saline (>34 psu) bottom waters from the south are deflected anticyclonically as they impinge on CYR. As expected, SST (Fig. 6c) is nearly isothermal in summer, masking mesoscale variations below. Under the stratified condition in summer, blocking exerted by CYR is mostly confined to depths (Jan et al., 1994).

2.4. Fall emergence of China Coastal Water

The onset of northeast monsoon leads to the emergence of CCW in the northwestern reaches. This is clear from temperature distribution at 10 m depth (Fig. 5d) and SST image (Fig. 6d). In upper depths, low-salinity waters (<33.5 psu) from Penghu Channel continue to intrude northward in fall. In consequence, zonal gradients of temperature and salinity begin to increase in the middle reaches of the strait (Jan et al., 1998). Winter blocking (Fig. 5a) can be fully established in about 2 months after the onset of northeast monsoon, completing the annual cycle.

3. Circulation modeling

The preceding observations tell a simple story which can be easily explained by known physics. In winter, the tendency of the Kuroshio Branch Current (Chu, 1971) to intrude northward over and beyond CYR is mostly halted by the northeast monsoon. The reduction in wind-induced blocking in spring unleashes the northward intrusion. Two modes of intru-

sion are conceivable. One skirts around CYR anticyclonically to conserve potential vorticity, similar to the model response in Chao (1994). The other branch hugs the coast of Taiwan similar to an internal bore intrusion along a coast (Stern et al., 1982). In consequence, a much broadened or bifurcated northward intrusion over CYR is likely. In summer, the Kuroshio Branch Water in the Penghu Channel is replaced by South China Sea Water due to changes in large-scale circulation pattern (Chao et al., 1996), and the northward intrusion is aided by the southwest monsoon. Under summer stratification. the ridge (CYR) is expected to manifest a stratified Taylor column (Hogg, 1973) in which the anticyclonic deflection of northward intrusion should be mostly confined to the bottom layer. The reduced topographic deflection arises from stratification and is commonly known as the Joint Effect of Baroclinicity and Bottom Relief or JEBAR. See Sarkisyan and Ivanov (1971) or Mertz and Wright (1992) for the mathematical expression of JEBAR and Isobe (2000) for an illustration of the consequent reduction in topographic steering. We will also illustrate the reduction of topography steering by stratification under summer conditions in Appendix A, after the main features of numerical results are discussed. The southwest monsoon also impedes the southward intrusion of China Coastal Water into the TS (Chao, 1990). Fall marks the beginning of wind-induced blocking of northward current on the eastern side; the China Coastal Water begins to emerge in the northwestern reaches of the TS with the aid of northeast monsoon.

Dynamical processes as outlined above are quite robust and can be easily captured by a host of existing numerical models. At this time, the scarcity of data set on the western side of TS presents problems to impose open-ocean boundary conditions that are needed to drive a model. The problem is generic in ocean modeling and a little reconnaissance effort is needed to rectify it. Nevertheless, the model-derived circulation is quite robust and insensitive to minor tuning in boundary forcing. To verify and to gain more insight, the general circulation model of Semtner (1986) is used below. The model contains a rigid lid and is formulated under Boussinesq and hydrostatic approximations. The three-dimensional model solves for temperature, salinity and velocities in three dimensions. The model domain is delineated in Fig. 1, with solid and dashed lines representing solid and open boundaries, respectively. The model resolution is 5 km horizontally and 10 m vertically. Horizontal and vertical mixing coefficients are set to 2.5×10^6 and 5 cm^2/s, respectively. Our insistence to use constant vertical mixing coefficient is based on the belief that the dominant mechanism is quite robust and should not depend on a particular turbulence closure scheme. After some preliminary tuning, it was determined that a choice of 5 cm^2/s produces the best overall agreement with the observed temperature and salinity fields.

At the sea surface, monthly wind stress as shown in Fig. 2 and seasonal heat flux derived from Hirose et al. (1999) are prescribed. Both wind stress and heat fluxes are spatially uniform, varying only in time. Salinity flux is set to zero at the sea surface. At the ocean bottom, heat and salinity fluxes are zero and a quadratic bottom stress is used with a nondimensional drag coefficient of 0.005.

In modeling mesoscale regions with expansive open-ocean boundaries, the choice of open-ocean

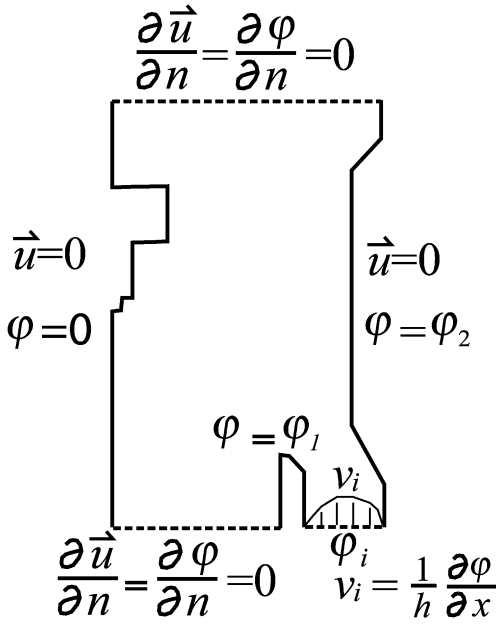

Fig. 7. Boundary conditions for velocities (u, v) and transport stream function (φ) on the solid and open boundaries. Inflow profiles for current (v_i) and stream function (v_i) are specified across Penghu Channel. Local water depth is h.

boundary conditions usually depends on the relative importance of remote versus local forcing. If local wind forcing dominates, no inflow or outflow is necessary to reproduce essential features of the circulation. Earlier observations as discussed in the preceding section clearly indicate the importance of remote forcing from areas outside the TS. Consequently, the inflow and outflow must be prescribed to a certain extent despite inadequate observations. In this light, the prescription of inflow and outflow cannot be completely objective and must be guided by limited observations. In terms of remote forcing, what stands out most from observations is the persistent northward inflow in the Penghu Channel in all seasons. Point current-meter measurements support the foregoing claim (Chuang, 1985, 1986). Hydrographic charts shown in Xiao and Cai (1988), China Ocean Press (1992), Wang and Chern (1988, 1992) as well as satellite-derived ocean color images in summer indicate more or less zonal isotherms and isohalines to the west of Penghu Channel. To the contrary, isotherms and isohalines become mostly meridional in the Penghu Channel. This evidence suggests preferable inflow through Penghu Channel. Recent Acoustic Doppler Current Profiler (ADCP) measurements by Jan and Chao (2002) lend further support to the persistent inflow through the Penghu Channel. These measurements were taken from 1999 to 2001; tidal currents were filtered out through repeated measurements at each station. In fact, the northward transport measured in the Penghu Channel follows an annual cycle very similar to that to be imposed in this model, peaking in summer and decreasing to minimum in winter months. We there-

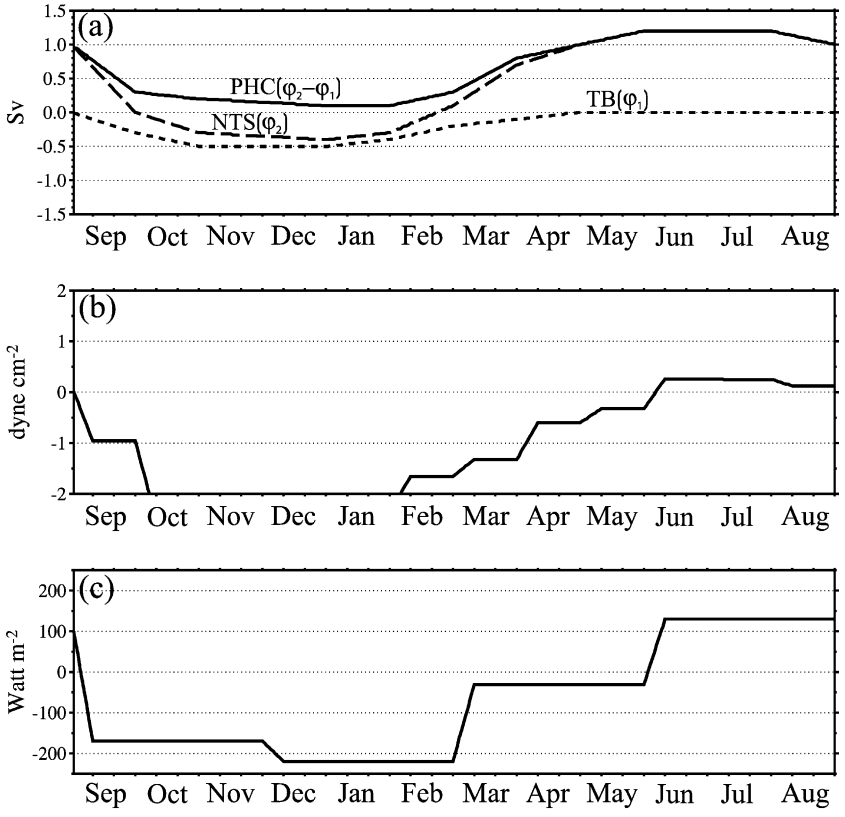

Fig. 8. The model input of annual cycle of (a) flow volume transport through the Penghu Channel (PHC), the Taiwan Banks (TB), and the northern Taiwan Strait (NTS); (b) sea surface wind stress; and (c) sea surface heat flux. Positive values are northward for volume transports and wind stress, and heat gains for the ocean.

fore prescribe a persistent inflow in the Penghu Channel while allowing transports through other parts of open boundaries to be loosely constrained by the climatological estimates of Wyrtki (1961). Regardless of our choice in open boundary conditions, the ultimate challenge for the chosen inflow and outflow is to reproduce essential features of observed temperature and salinity fields in the strait. With this goal in mind, we have adjusted the seasonal variation of inflow through the Penghu Channel.

Fig. 7 illustrates boundary conditions for currents and depth-integrated stream function (φ) on land and open-ocean boundaries. These conditions are chosen to minimize over-specification of inflow–outflow profiles and locations. Land boundaries are no-slip. Inflow location is fixed only in the Penghu Channel. The depth-averaged current (v_i) entering Penghu Channel varies in time, but its profile in the cross-stream direction remains similar. The baroclinic portion of Penghu Channel inflow is not fixed. Rather, it is extrapolated from adjacent interior by assuming zero normal gradients. Except for the Penghu Channel inflow, all other inflow and outflow locations are not specified a priori. By imposing zero normal gradients for currents on open boundaries, inflow–outflow locations are largely determined by flow fields in the interior of model domain.

Boundary conditions for stream function fix volume transports through the strait. The stream function is specified for the Penghu Channel inflow as φ_i. Elsewhere, the stream function varies only in time on solid boundaries, and has zero gradient normal to an open-ocean boundary. By doing so, the total volume transport in the strait is φ_2. It is also clear from Fig. 7 that the northward transport is φ_1 west of Penghu Island, and $\varphi_2 - \varphi_1$ east of it.

Throughflow transports are fixed around estimates given by Wyrtki (1961). On southern boundaries, partition of volumetric fluxes between east and west of Penghu Islands (see Fig. 1) requires tuning. Being guided by observations, we impose a persistent but seasonally varying inflow in the Penghu Channel, peaking in summer but decreasing to minimum in winter. Being blocked by the Taiwan Banks to the south, wind-driven transport through the open boundary west of Penghu Islands is significant only in winter. Fig. 8 shows the estimated transports through three open boundaries, along with the monthly wind

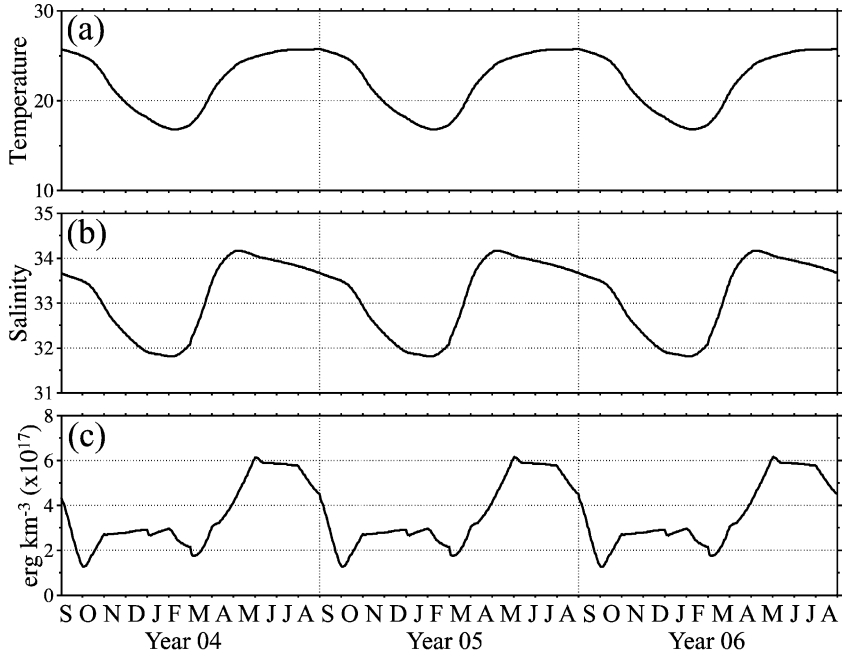

Fig. 9. Model-produced time series of volume-averaged (a) temperature, (b) salinity and (c) kinetic energy from year 4 to year 6.

stress and seasonal air–sea heat flux used in the model. The transport estimates are optimized to produce reasonable agreement with observed hydrography, and to conserve total heat content inside the strait on interannual time scales. Further, abrupt changes in monthly wind stress and quarterly heat flux are smoothed linearly.

Temperature and salinity on open boundaries are subject to advection by the normal flow. Incoming temperature and salinity are prescribed for inflows, varying bimonthly according to observations. A challenge in imposing open boundary temperature and salinity is to reproduce the China Coastal Current in the western reaches of the strait (China Ocean Press, 1992). Data scarcity on the western side of the strait presents problems to prescribe inflow temperature and salinity for the China Coastal Water in winter. The problem is not serious; model-derived circulation patterns are quite robust and insensitive to the property of China Coastal Water. However, minor tuning does improve model-data agreement. In this light, satellite-derived sea surface temperature for the China Coastal Water is projected into the water column by assuming a vertical profile similar to that of surrounding waters. Salinity for the China Coastal Water is similarly projected into the water column using surface values reported by Xiao and Cai (1988).

An initial condition is needed before driving the model to a steady annual cycle. To achieve this, the basin is first filled with homogeneous and motionless seawater. The summer climatological forcing at open-ocean boundary and air–sea interface is then held steady to drive the system for 200 days. Thereafter, the system becomes steady. Subsequently, the summer equilibrium state is used as the initial condition. Seasonally varying forcing is then imposed for 6 years to drive the basin to a steady annual cycle. Fig. 9 shows time series of basin-averaged temperature, salinity and kinetic energy from year 4 to year 6. The steady seasonal cycle is clearly established after the fourth year. Results from year 6 are discussed below. Since external forces used to drive the system are mostly seasonal, solutions vary little on a monthly time scale. In this light, a particular choice of the day for illustrations below is not important; any other choice in the same month would produce visually indistinguishable results.

4. Model results

4.1. Winter circulation

Fig. 10 shows near-surface (top panels) and near-bottom (bottom panels) features on January 1 of the sixth year. Temperature and flow fields are shown in left panels while corresponding salinity patterns are shown in right panels. Flow fields are superimposed on left panels only. The blocked circulation pattern in winter is reproduced. Moving against the winter northeast monsoon, the Kuroshio Branched Current entering from Penghu Channel is mostly blocked by the Changyun Rise (CYR), turning southward and leaving the strait. A small portion manages to flow northward over and beyond the CYR. The China Coastal Water is colder (<20 °C) and fresher (<32 psu), moving southward along the western boundary of the strait. Partial blocking around the CYR is evident, as a part of the China Coastal Water turns back northward at the expense of southward intrusion. Features at 15 and 45 m are similar, indicating the barotropic nature of winter circulation. Further, temperature and salinity distributions are quite similar to the observed patterns in Figs. 5 and 6. In the northwestern reaches of the basin, currents appear to leave the coast of China from 15 m down. The eastward flow is mostly fed by a westward Ekman drift in the top 10 m of the water column (not shown). Note that the wind is from northeast in January (Fig. 2), driving an essentially westward surface Ekman drift.

Note also the establishment of a zonal front near the CYR in the near-surface temperature and salinity fields (Fig. 10a and b). This zonal front is rather persistent in winter from hydrographic observations (Fig. 5a). Apparently, a zonal front is a dynamic barrier against northward transport. Blocking by the CYR is crucial for the establishment of the zonal front. In fact, the winter circulation of the TS was examined earlier by Jan et al. (1998) using a similar numerical model. In that study, the winter circulation was obtained by maintaining constant climatological forcing, inflow and outflow typically encountered in winter. The final steady-state solution derived from that model is quite similar to Fig. 10. The present model is an extension of the earlier model by including seasonal variations. In Jan et al. (1998), model simulations with and without the CYR were exam-

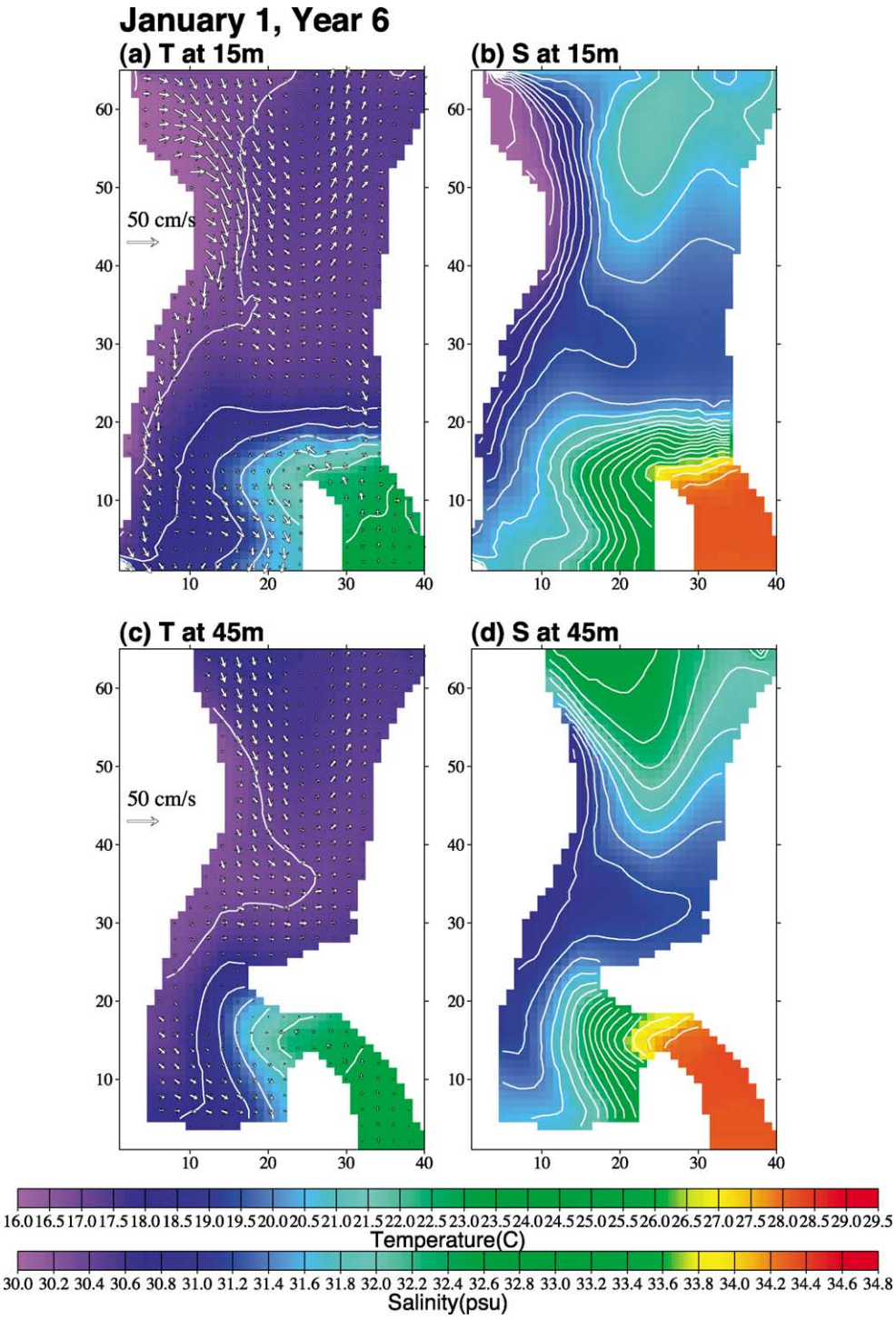

Fig. 10. Model-produced (a) temperature at 15 m, (b) salinity at 15 m, (c) temperature at 45 m and (d) salinity at 45 m on January 1 of the sixth year. Also imposed on panels (a) and (c) are flow fields at corresponding depths. Arrows are plotted at every other grid. Color bars for temperature and salinity are attached on bottom. Horizontal scales are in units of horizontal grid spacing.

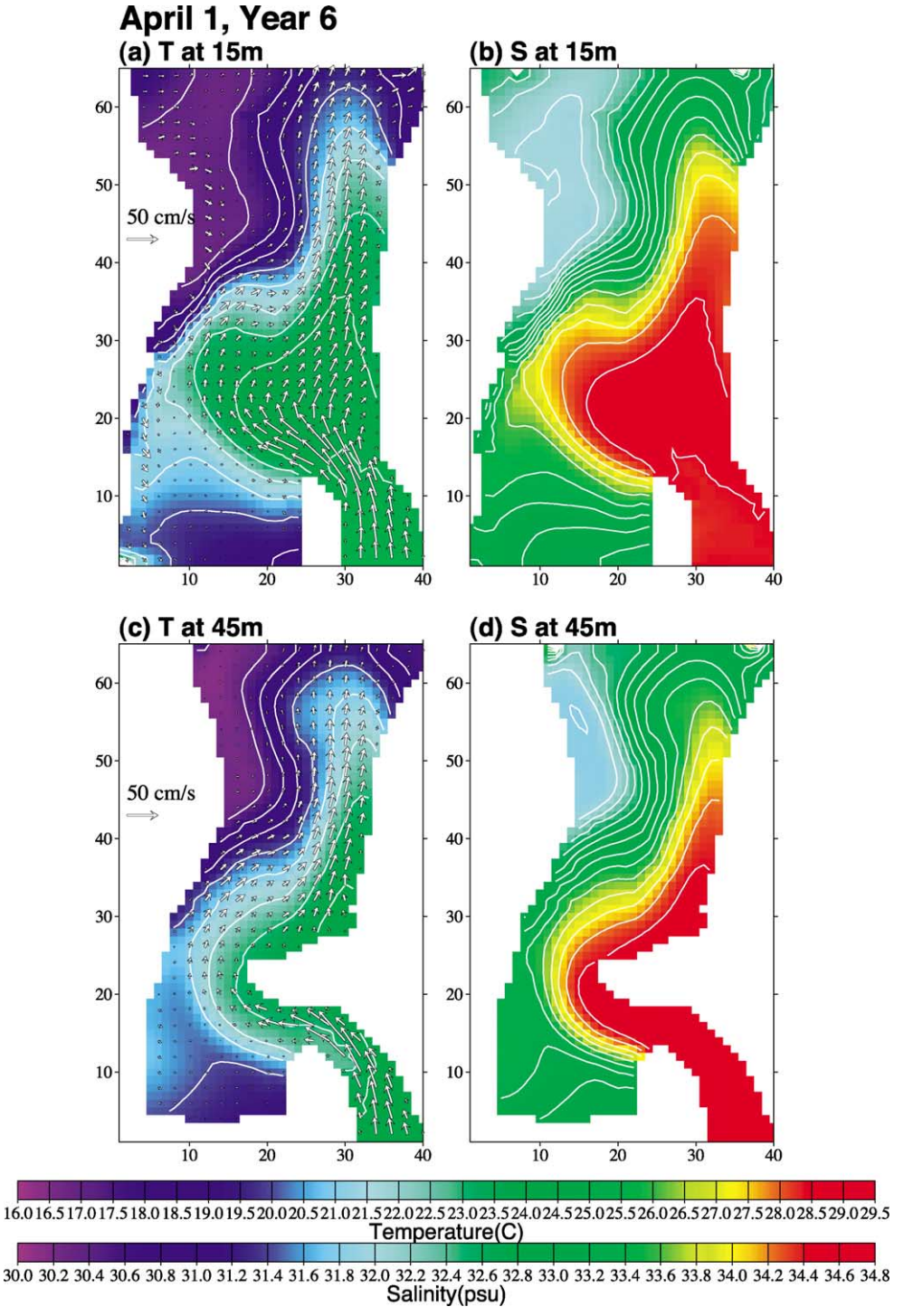

Fig. 11. Same as Fig. 10 but on April 1 of the sixth year.

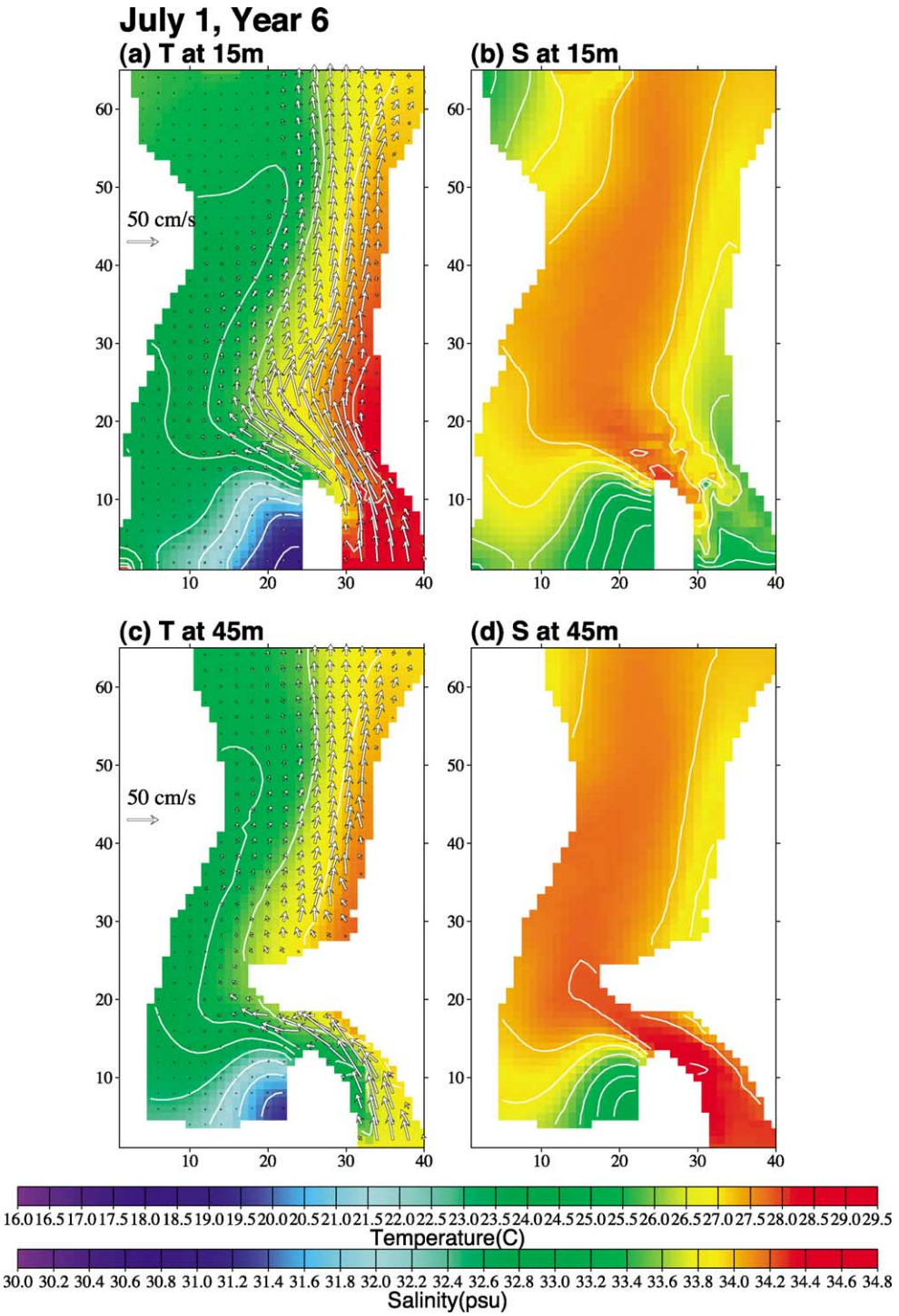

Fig. 12. Same as Fig. 10 but on July 1 of the sixth year.

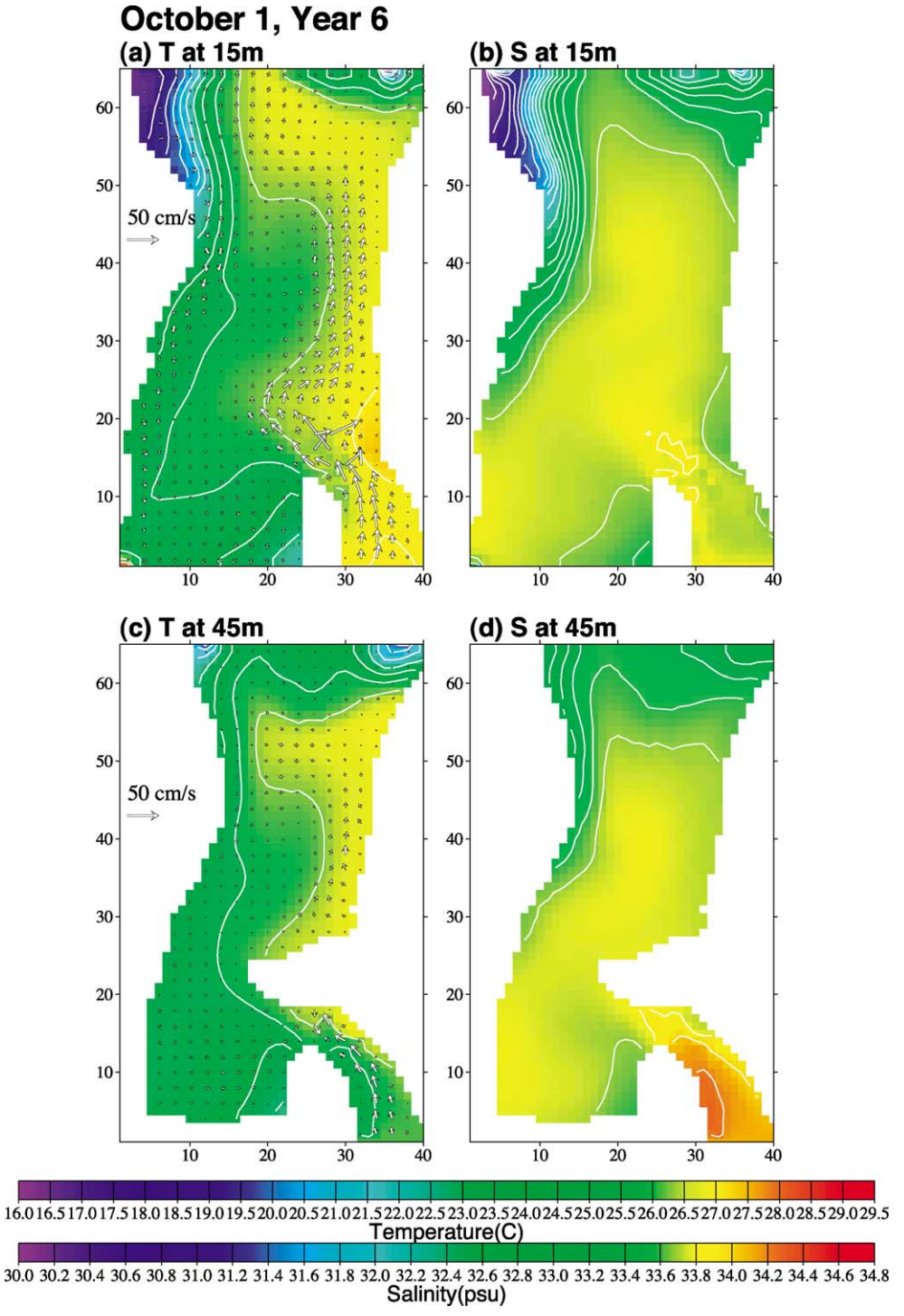

Fig. 13. Same as Fig. 10 but on October 1 of the sixth year.

ined. Without the CYR, the zonal front virtually disappeared; isotherms and isohalines become more or less oriented in the north–south direction. However, the removal of the CYR will not fully eliminate winter blocking, because the northeast monsoon is still able to retard the northward intrusion of Kuroshio water. Nevertheless, blocking by winds alone is not as effective without the aid of the CYR in winter. The northward intrusion of Kuroshio water against the winter northeast monsoon is far greater if the CYR is removed.

4.2. Spring circulation

Fig. 11 shows model-derived circulation, temperature and salinity on April 1 of the sixth year. The spring relaxation of northeast monsoon unleashes the once-blocked northward intrusion of Kuroshio Branched Water in winter. The inflow from Penghu Channel turns anticyclonically over the CYR, narrowing once more in the northern reaches of the strait. The much broadened northward current over the CYR actually bifurcates slightly near surface (top left panel); one branch follows the flank of the CYR and the other tends to follow the coast of Taiwan. The northward intrusion reduces the penetration distance of the China Coastal Water. Both temperature and salinity fields show northward retreat of the China Coastal Water from its winter extent. Circulation in spring is still fairly barotropic; surface and bottom features are quite similar. The modeled temperature and salinity fields compare favorably with observations (Figs. 5 and 6).

4.3. Summer circulation

Fig. 12 shows surface and bottom features on July 1 of the sixth year. With the aid of summer stratification and southwest monsoon, the northward intrusion in summer is almost unimpeded by the CYR. For the surface northward flow, the anticyclonic deflection by the CYR is much reduced because of stratification. In consequence, the surface current attains speeds as high as 150 cm/s over the CYR because of shoaling of bottom topography. Temperature and salinity fields are relatively featureless, as one would expect from a summer isothermal environment. Note also that the inflow from Penghu Channel carries warmer and fresher South China Sea Water instead of the Kuroshio Branch Water in summer. The contributions of summer stratification and bottom obstacle (CYR) to the summer circulation pattern will be further illustrated in Appendix A.

4.4. Fall circulation

Fig. 13 shows near-surface and near-bottom features on October 1 of the sixth year. With the arrival of northeast monsoon, the northward intrusion current over and beyond the CYR is much reduced in strength. Further, downwind acceleration allows the colder and fresher China Coastal Water to reappear in the northwestern reaches of the strait. Between the northward current on the east side and southward flow on the west side, a cyclonic eddy is formed north of the CYR. The cold eddy, becoming colder in time as the season progresses, is still in the early stage of development. This eddy in its mature stage was observed earlier by Wang and Chern (1989). As winter approaches, the northward current on the east side will be blocked by CYR and the China Coastal Waters on the west side will penetrate farther southward (see Fig. 10), completing the annual cycle.

5. Summary

A recent hydrography data set, SST imagery and a numerical ocean model are used to derive seasonal circulation in the TS. The historical description about the strait throughflow is inadequate, lacking mesoscale variability induced by a ridge (CYR) in the middle reaches of the strait. The topography-forced circulation comes to light after 5 years of observational efforts from 1985 to 1989. Satellite-derived SST images provide additional reality check. The numerical model verification lends further support. At the present time, the climatological data set still lacks details especially in the western reaches of the strait. In consequence, open-ocean boundary conditions are not adequately resolved. The present model utilized a little ‘‘reconnaissance’’ effort to make up the deficiency. Fortunately, the circulation patterns are quite robust and highly reproducible by the numerical model, despite the inadequacy in open-ocean boundary forcing.

Fig. 14 illustrates schematically circulation patterns in four seasons, summarizing this investigation. In winter (Fig. 14a), the northward intrusion of Kuroshio Branch Water is severely blocked by the northeast monsoon, and the southward penetration of China Coastal Water is maximum. A portion of the China Coastal Water is deflected by the CYR and turns back northeastward. In spring (Fig. 14b), relax-

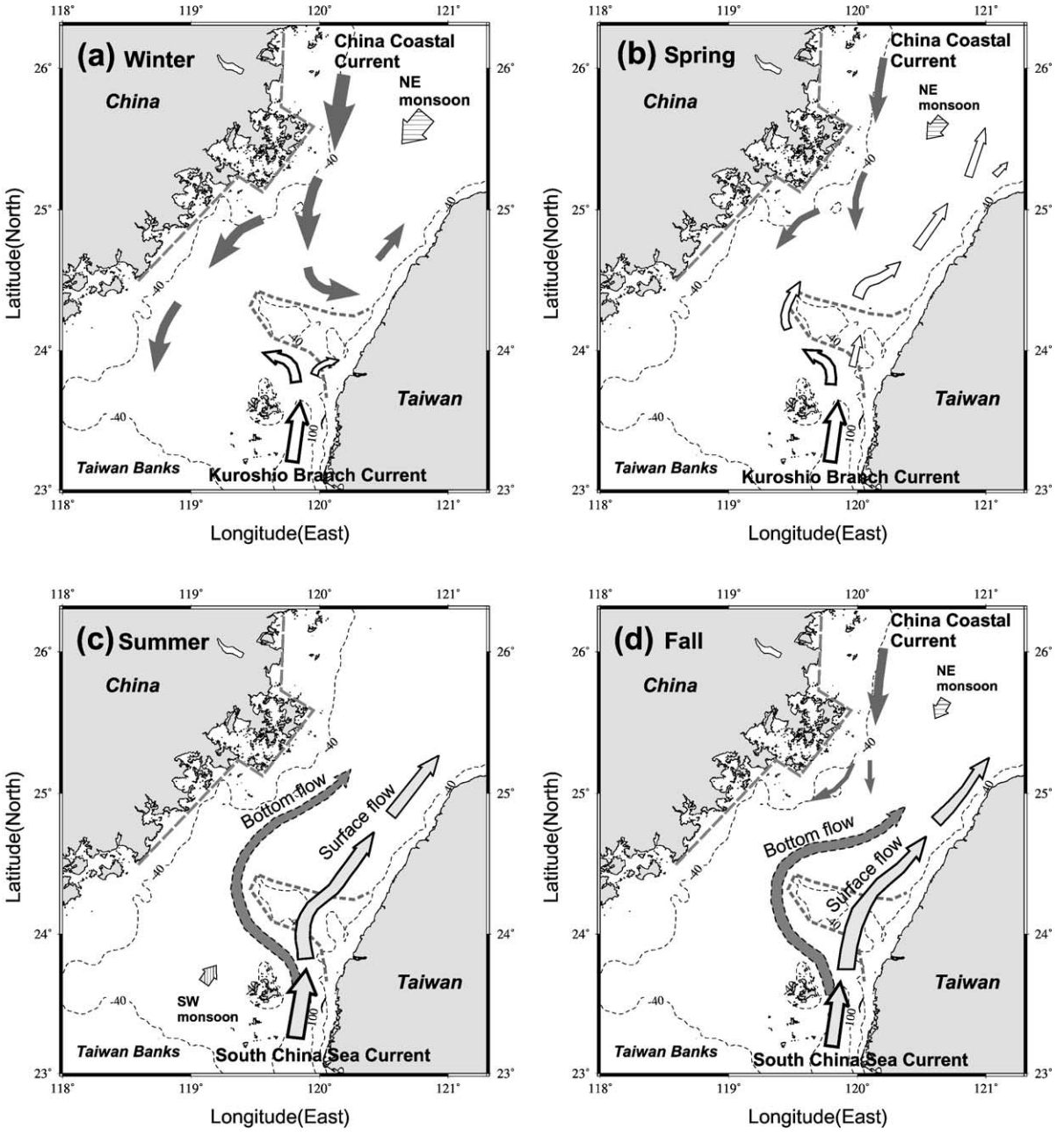

Fig. 14. Schematic showing the Taiwan Strait circulation in (a) winter, (b) spring, (c) summer and (d) fall. A thick and short-dashed line marks the outer edge of Changyun Rise. A thick and long-dashed line illustrates the deflection by the China coast.

ation of northeast monsoon unleashes the northward intrusion of the Kuroshio Branch Water, and the China Coastal Water retreats northward. With the aid of summer stratification and southwest monsoon, the northward intrusion of the South China Sea Water in summer (Fig. 14c) is relatively unimpeded by the

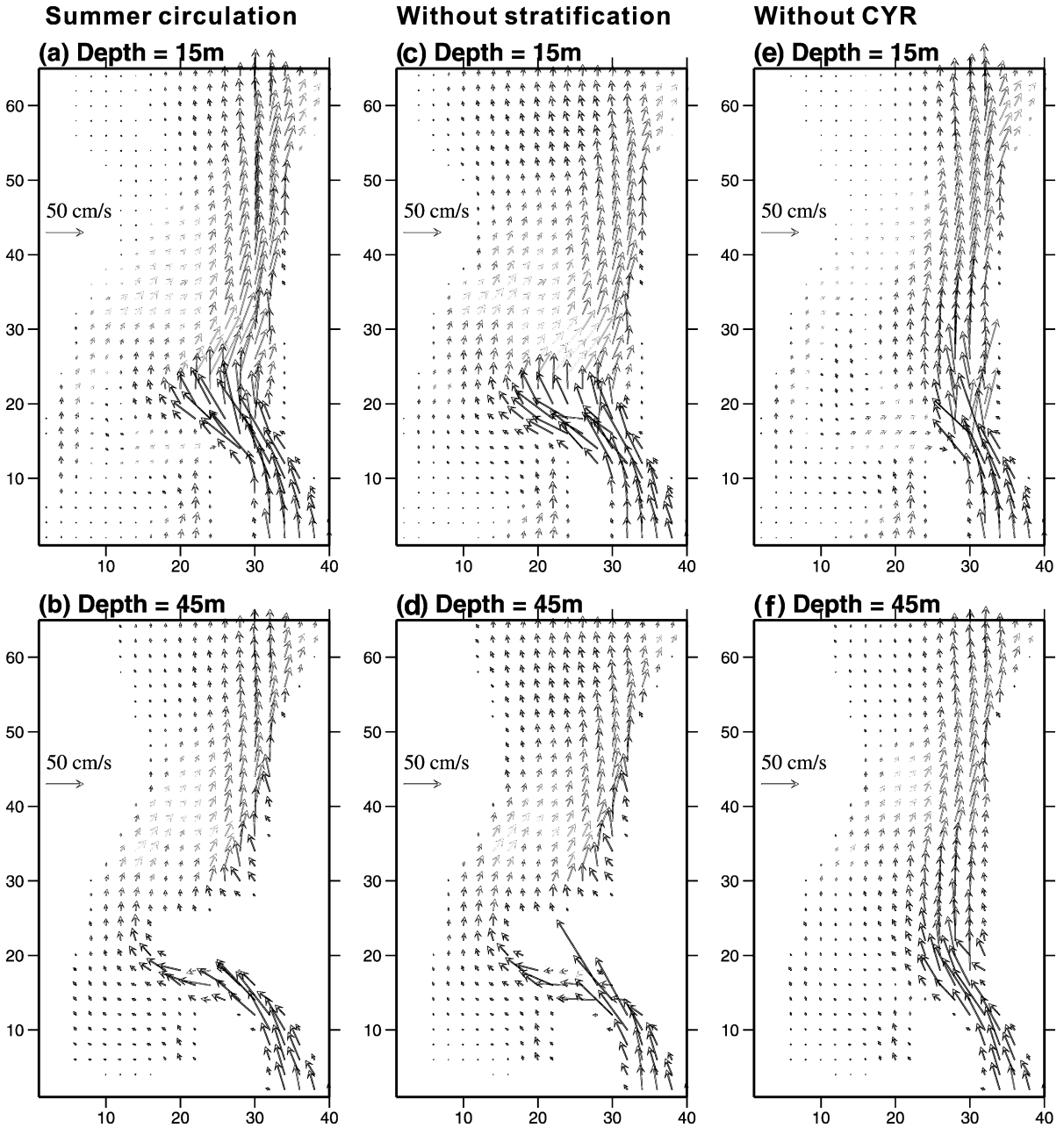

Fig. 15. Model-derived summer flow fields at 15 m depth (top panels) and 45 m depth (bottom panels). Left panels (a and b) include both summer stratification and Changyun Rise. Middle panels (c and d) are the corresponding solutions if the summer stratification is removed. In the right two panels (e and f), Changyun Rise is removed but the summer stratification is retained.

CYR; only the bottom flow is deflected anticyclonically. Further, the China Coastal Water fails to enter the TS. The fall pattern (Fig. 14d) is similar to the summer pattern, except for the emergence of the China Coastal Water in the northwestern reaches of the strait.

The foregoing discussion of the TS circulation is limited to the seasonal time scale. Circulation patterns below and beyond the seasonal time scale remain to be elucidated. Below the seasonal time scale, the effect of typhoons in the fall season is particularly noteworthy. Beyond the seasonal time scale, the effect of El Niño is expected to modulate the strait circulation on interannual time scales. Although the TS is quite remote from major areas impacted by El Niño, the signature of El Niño on the local weather is unmistakable. Its effect on the TS needs to be examined. In light of these complexities, the present study serves only as a modest beginning toward a long line of future investigations.

Acknowledgements

Professor M.-A. Lee of National Taiwan Ocean University kindly provided satellite remote-sensing sea surface temperature data. Anonymous reviewers contributed substantially to the improvement of this paper. This is the National Center for Ocean Research (NCOR) of Taiwan, contribution number 25.

Appendix A. Effects of stratification and bottom obstacle on summer circulation

Focussing on the summer circulation, the effect of the Changyun Rise (CYR) and summer stratification on the northward intrusion current is investigated below. In these simulations, the climatological forcing (including wind stress and surface heat flux) at the sea surface and open-boundary inflow and outflow are fixed at their summer conditions. The initial strait water is motionless. If summer stratification is included, the initial stratification is the mean stratification averaged over the entire strait area. For the barotropic simulation, the specification of surface heat flux and inflow temperature and salinity is not necessary. Simulations were carried out for 60 model days, driving solutions to steady states appropriate for the summer condition.

Fig. 15 shows three solutions at 15 m depth (top panels) and 45 m depth (bottom panels). The left two panels (a and b) are from the all-inclusive experiment. In the middle two panels (c and d), summer stratification is removed and the solution is barotropic. In the right two panels (e and f), the CYR is removed but the stratification is retained. For simplicity, only flow fields are shown in Fig. 15.

Using the all-inclusive solution in the left two panels as a reference, the effects of stratification and bottom obstacle (CYR) are evident. If the summer stratification is removed, the anticyclonic deflection of surface currents around the CYR is more pronounced (Fig. 15c). In other words, the topographic influence is no longer confined to near the bottom but extends to the surface in the absence of stratification. Thus, the typical summer stratification is strong enough to suppress the upward expansion of bottom anticyclonic vorticity induced by the CYR. This bahavior is consistent with existing theories (Hogg, 1973; Isobe, 2000). If the bottom obstacle (CYR) is removed, the anticyclonic deflection of the northward current is mostly absent (Fig. 15e and f) as expected. In this case, the northward current hugs the coast of Taiwan and behaves like a Kelvin wave.

References

Chao, S.-Y., 1990. Circulation of the East China Sea, a numerical study. Journal of the Oceanographic Society of Japan 46, 273–295.

Chao, S.-Y., 1994. Zonal jets over topography on a beta-plane, with applications to the Kuroshio Extension over the Shatsky Rise. Journal of Physical Oceanography 24, 1512–1531.

Chao, S.-Y., Shaw, P.-T., Wu, S.Y., 1996. Deep water ventilation in the South China Sea. Deep-Sea Research 43, 445–466.

China Ocean Press, 1992. Marine Atlas of Bohai Sea, Yellow Sea and East China Sea Hydrology, Beijing, 524 pp.

Chu, T.-Y., 1971. Environmental study of the surrounding waters of Taiwan. Acta Oceanographica Taiwanica 1, 15–32.

Chuang, W.-S., 1985. Dynamics of subtidal flow in the Taiwan Strait. Journal of the Oceanographic Society Japan 41, 65–72.

Chuang, W.-S., 1986. A note on the driving mechanisms of current in the Taiwan Strait. Journal of the Oceanographic Society Japan 42, 355–361.

Fang, G., Zhao, B., Zhu, Y., 1991. Water volume transport through the Taiwan Strait and the continental shelf of the East China Sea

measures with current meters. In: Takano, K. (Ed.), Oceanography of Asian Marginal Seas. Elsevier, New York, pp. 345–358.

Guan, B., 1994. Patterns and structures of the currents in Bohai, Huanghai and East China Seas. In: Zhao, D., Liang, Y.-B., Zeng, C.-K. (Eds.), Oceanology of China Seas, vol. 1. Kluwer Academic Publishers, Dordrecht, Netherlands, pp. 17–26.

Hirose, N., Lee, H.-C., Yoon, J.-H., 1999. Surface heat flux in the East China Sea and the Yellow Sea. Journal of Physical Oceanography 29 (3), 401–417.

Hogg, N.G., 1973. On the stratified Taylor column. Journal of Fluid Mechanics 58, 517–537.

Huang, Q., Wang, W., Li, Y.S., Li, C.W., 1994. Current characteristics of the South China Sea. In: Zhao, D., Liang, Y.-B., Zeng, C.-K. (Eds.), Oceanology of China Seas, vol. 1. Kluwer Academic Publishers, Dordrecht, Netherlands, pp. 17–26.

Ishii, T., Kondo, J., 1987. Seasonal variation of the heat balance of the East China Sea. Tenki 34, 517–526 (in Japanese).

Isobe, A., 1999. On the origin of the Tsushima warm current and its seasonality. Continental Shelf Research 19, 117–133.

Isobe, A., 2000. Two-layer model on the branching of the Kuroshio southwest of Kyushu, Japan. Journal of Physical Oceanography 30, 2461–2476.

Jan, S., Chao, S.-Y., 2002. Seasonal variation of volume transport in the major inflow channel of the Taiwan Strait: Penghu Channel. Deep-Sea Research II, in press.

Jan, S., Chern, C.-S., Wang, J., 1994. A numerical study on currents in Taiwan Strait during summertime. La mer 32 (4), 225–234.

Jan, S., Chern, C.-S., Wang, J., 1998. A numerical study of currents in the Taiwan Strait during winter. Terrestrial, Atmospheric and Oceanic Sciences 9, 615–632.

Kalnay, E., et al., 1996. NCEP/NCAR 40-year reanalysis project. Bulletin of American Meteorological Society 77, 437–471.

Levitus, S., 1982. Climatological atlas of the world ocean. NOAA Professional Paper no. 13. US Government Printing Office, Washington, D.C., 173 pp.

Mertz, G., Wright, D.G., 1992. Interpretation of the JEBAR term. Journal of Physical Oceanography 22, 301–305.

Na, J., Seo, J., Lee, H.-J., 1999. Annual and seasonal variations of the sea surface heat fluxes in the East Asian marginal seas. Journal of Oceanography 55, 257–270.

Ninno, H., Emery, K.O., 1961. Sediments of shallow portions of East China Sea and South China Sea. Geological Society of America Bulletin 72, 731–762.

Nitani, H., 1972. Beginning of the Kuroshio. In: Stommel, H., Yoshida, K. (Eds.), Kuroshio, Its Physical Aspects. University of Tokyo Press, Tokyo, pp. 129–163.

Sarkisyan, A.S., Ivanov, V.F., 1971. Joint effect of baroclinicity and bottom as an important factor in the dynamics of sea currents. Bulletin Academy of Science USSR, Atmospheric and Oceanic Physics (English translation) 7, 173–188.

Semtner, A.J., 1986. Finite difference formulation of a world ocean model. In: O'Brien, J.J. (Ed.), Proceedings of the NATO Advanced Study Institute on Advanced Physical Oceanographic Numerical Modeling. D. Reidel Publishing, Dordrecht, pp. 187–231.

Stern, M.E., Whitehead, J.A., Hua, B.-L., 1982. The intrusion of a density current along the coast of a rotating fluid. Journal of Fluid Mechanics 123, 237–265.

Wang, J., Chern, C.-S., 1988. On the Kuroshio branch in the Taiwan Strait during wintertime. Progressive Oceanography 21, 469–491.

Wang, J., Chern, C.-S., 1989. On cold water intrusions in the eastern Taiwan Strait during the cold season. Acta Oceanographica Taiwanica 22, 43–67.

Wang, J., Chern, C.-S., 1992. On the distribution of bottom cold waters in Taiwan Strait during summertime. La mer 30, 213–221.

Wyrtki, K., 1961. Physical oceanography of the southeast Asia waters. Scientific results of marine investigations of the South China Sea and Gulf of Thailand. 1959–1961, Naga Report, 195 pp.

Xiao, H., Cai, S., 1988. Distribution characters of sea temperature and salinity in western Taiwan Strait. Journal of Oceanography in Taiwan Strait 7 (3), 227–234 (in Chinese).